Expanded View Figures

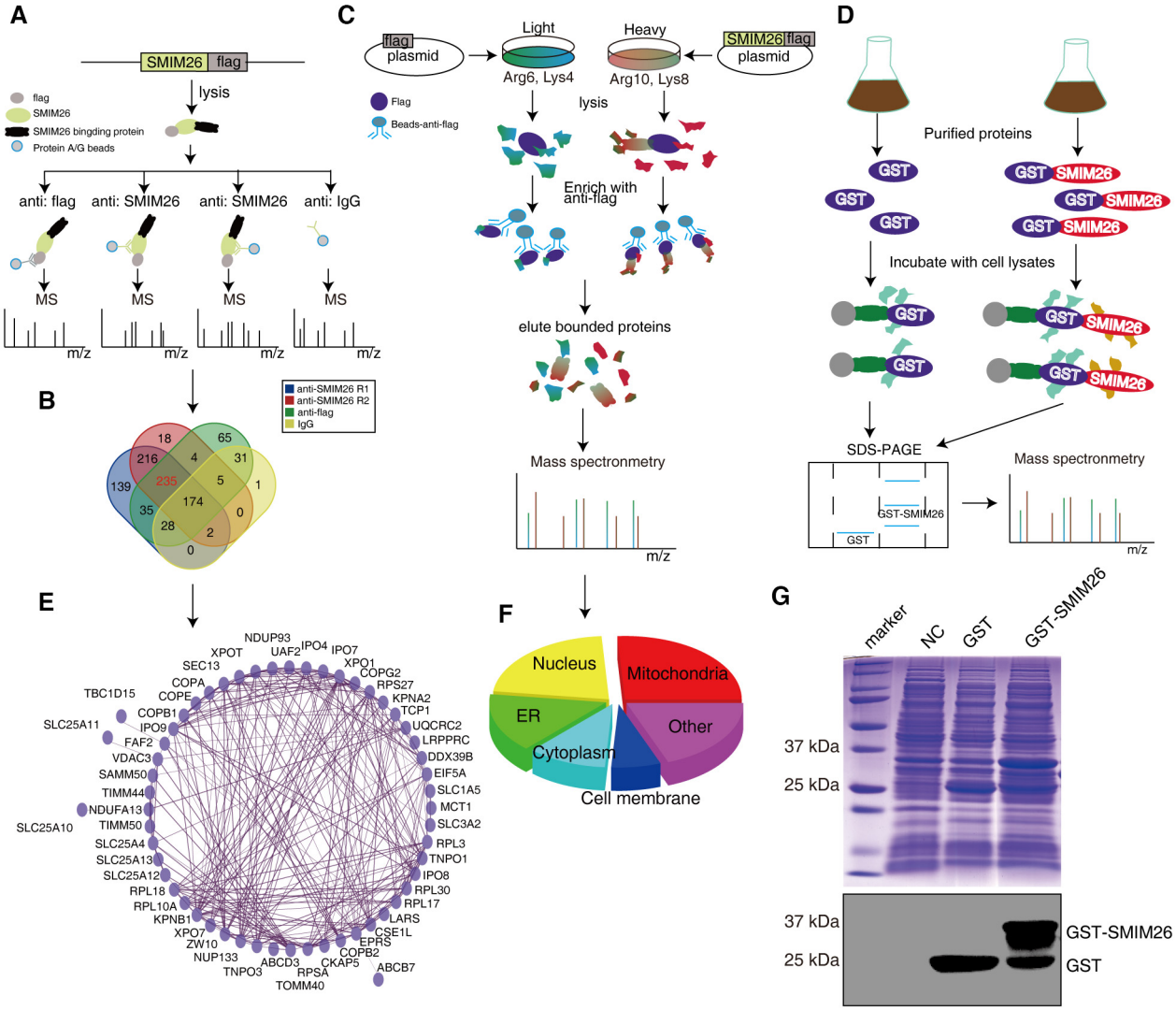

Figure EV1. The interaction network of SMIM26.

A The diagram depicting the workflow of identifying SMIM26-interacting proteins. The SMIM26-flag plasmid was transfected into HEK293T cells, anti-flag and anti-SMIM26 antibodies were used for immunoprecipitation, and anti-IgG was used as the control; the immunoprecipitated proteins were identified by mass spectrometry.

B Venn diagram showing 235 proteins potentially interacted with SMIM26.

C SILAC-CoIP was used to identify SMIM26-interacting proteins. HEK293T cells cultured in heavy medium (Arg10 and Lys8) or light medium (Arg6 and Lys4) were transfected with control plasmid or SMIM26-flag plasmid, respectively. After anti-flag antibody was used for immunoprecipitation, lysates were mixed and subjected to mass spectrometric analysis.

D The diagram showing the workflow of GST pulldown. GST and GST-SMIM26 expression were induced by IPTG and purified in prokaryotic cells BL21, then subjected to pulldown experiments with cell lysates, and the products were subjected to mass spectrometric analysis.

E The PPI network of SMIM26 was constructed by Cytoscape software.

F GO analysis (cellular components) of SMIM26 interacting proteins was shown in the pie chart.

G Coomassie blue staining showing the expression of GST-SMIM26 protein in BL21 cells was successfully induced by IPTG.

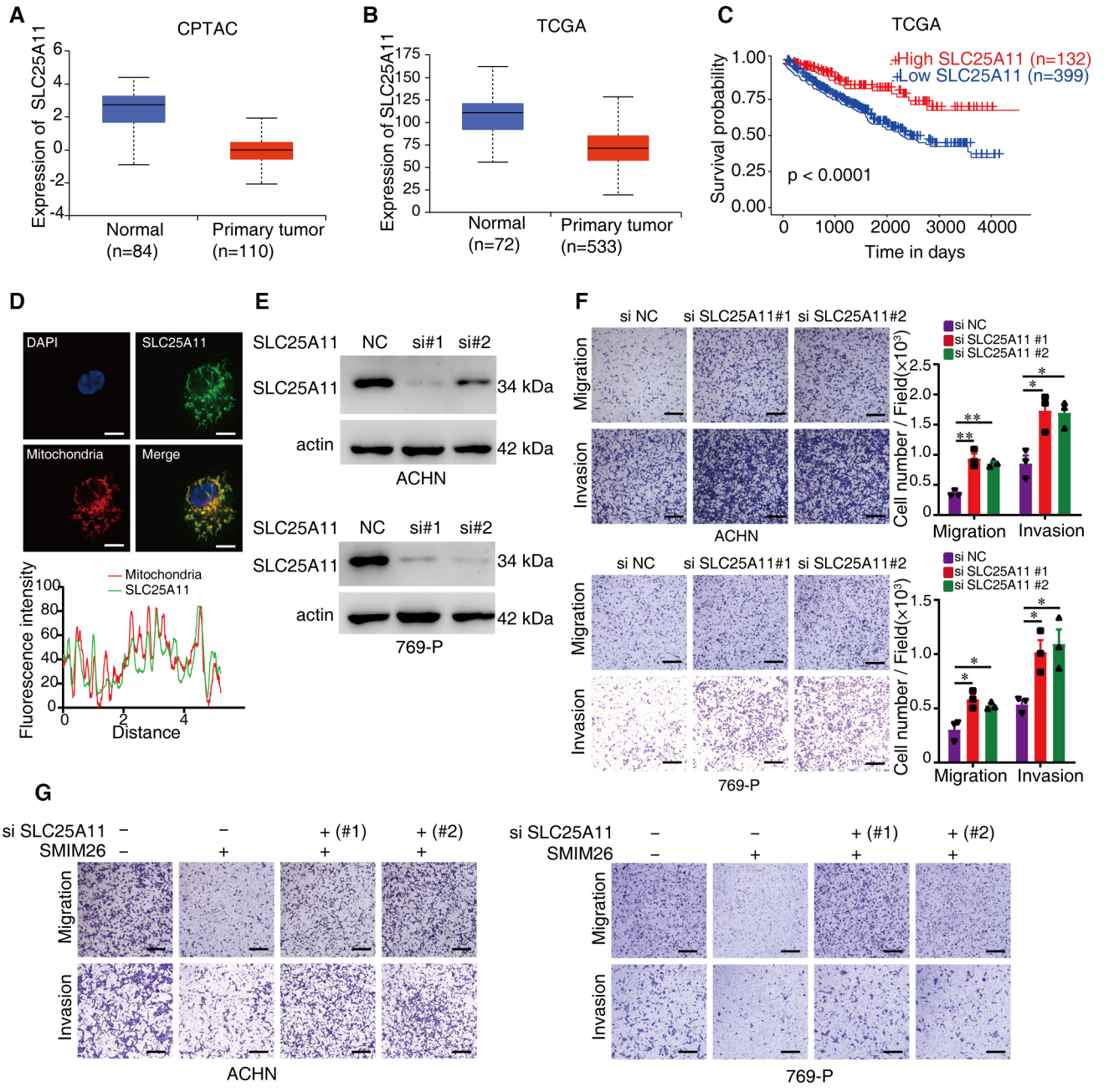

Figure EV2. SLC25A11 is a tumor suppressor in ccRCC.

A, B The comparisons of SLC25A11 expression in ccRCC tissue and normal tissue from CPTAC (A) and TCGA databases (B). The central lines reflect the median, and the bottom and top of the box represent the first and third quartiles, respectively. The whiskers reflect the min-to-max distribution of expression.

C The TCGA database depicts that the low expression of SLC25A11 is associated with a poor prognosis of ccRCC patients.

D Immunofluorescence of SLC25A11 (green) and mitochondria (red) in ACHN cells. Nuclei were stained with DAPI (blue). Scale bar, 10 μm.

E Immunoblotting validation of the knockdown effect of SLC25A11 in ACHN and 769-P cells.

F Migration and invasion abilities of ACHN and 769-P cells with or without knockdown of SLC25A11 were detected by transwell assays. Unpaired two-tailed Student's *t*-test, $*P < 0.05$, $**P < 0.01$. Scale bar, 600 μm. Data are shown as mean ± SEM of three biological replicates.

G Transwell assays were used to test the migration and invasion abilities of both ccRCC cells with indicated treatment. Scale bar, 600 μm.

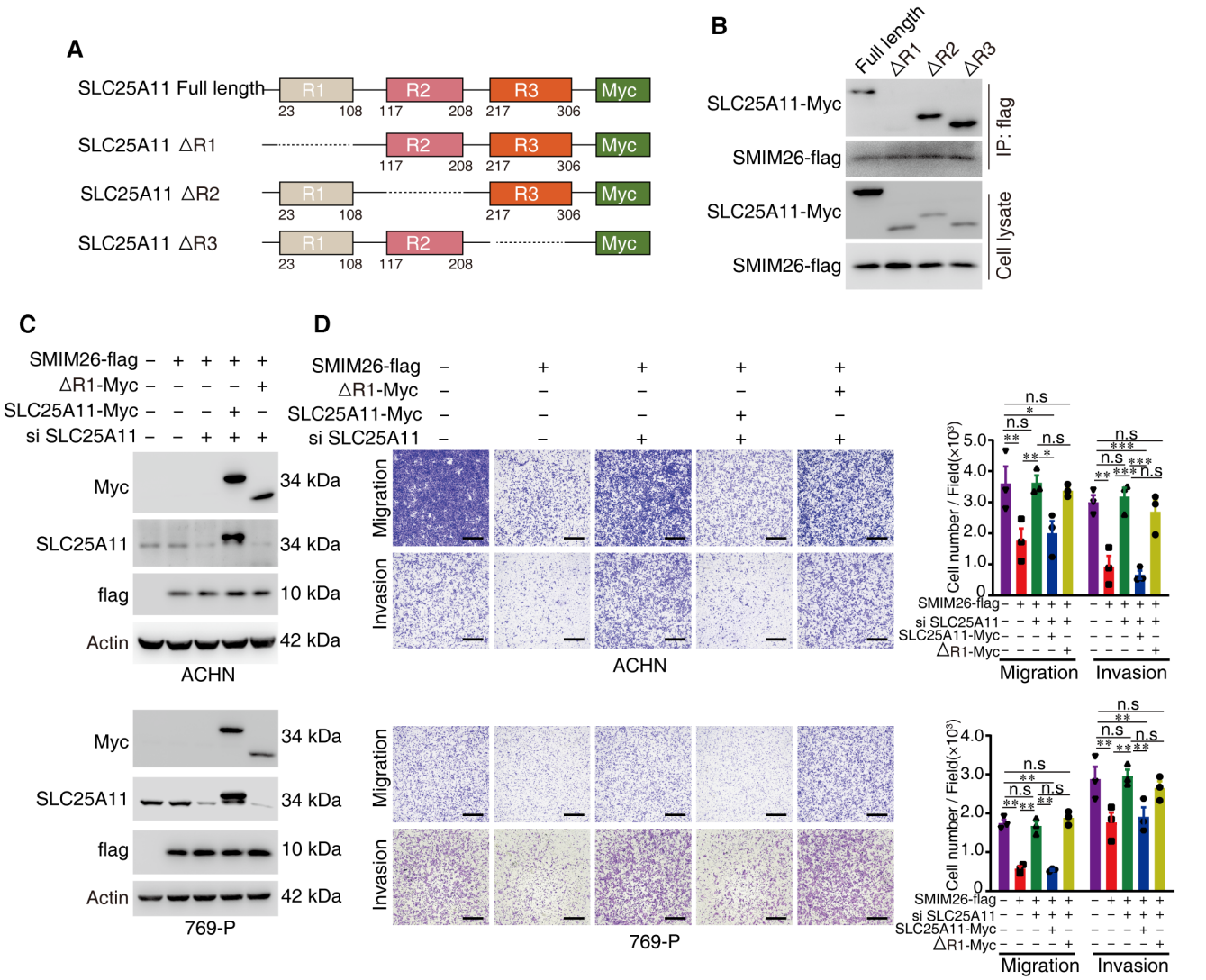

Figure EV3. SMIM26 inhibits ccRCC by binding to SLC25A11.

A Diagram of SLC25A11 wild-type and domain deletion mutation constructs.

B The indicated Myc-tagged wild-type and mutants of SLC25A11 were transfected with SMIM26-flag into HEK293T cells, and SMIM26-flag complexes were Co-IP by anti-flag antibody, truncated SLC25A11 and SMIM26-flag were then detected.

C Overexpression of wild-type and R1-domain deleted truncated SLC25A11 with SMIM26-flag in endogenously SLC25A11 knockdown ccRCC cells.

D Overexpression of wild-type SLC25A11 but not R1-domain deleted SLC25A11 in endogenous SLC25A11 knockdown ccRCC cells can restore the SMIM26-mediated inhibition of migration and invasion. Two-way ANOVA, $*P < 0.05$, $**P < 0.01$, $***P < 0.001$. n.s, non-significant. Scale bar, 600 μm. Data are shown as mean ± SEM of three biological replicates.

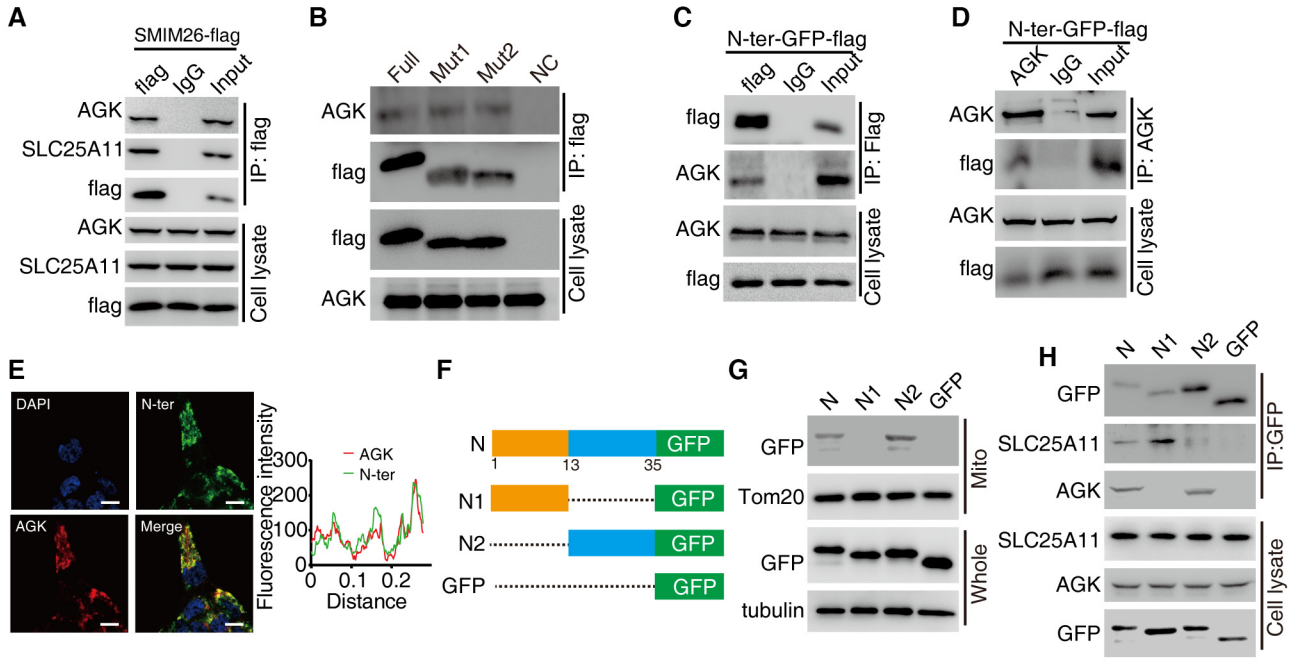

Figure EV4. SMIM26 interacts with AGK.

A CoIP assays were used to verify the interaction between exogenous SMIM26 and endogenous AGK in xenograft tumor samples.

B The indicated flag-tagged wild-type and mutants of SMIM26 were transfected into HEK293T cells, and SMIM26-flag complexes were Co-IP by anti-flag antibody, and AGK and SMIM26-flag were then detected.

C, D N-ter domain of SMIM26 fused with GFP-flag interacted with AGK. The N-ter SMIM26-GFP-flag construct was transfected into HEK293T cells, and co-immunoprecipitation was performed by using anti-flag antibody (C) and anti-AGK antibody (D).

E Immunofluorescence of N-ter SMIM26 (green) co-localized with AGK (red) in ACHN cells. Nuclei were stained with DAPI (blue). Scale bar, 10 μm. The red line of statistical analysis centers on the co-location of AGK (red) and N-ter of SMIM26 (green).

F Diagram of truncated N-ter SMIM26.

G CoIP assays indicated that N-ter of SMIM26 missing transmembrane domain (N1) lost the function of interaction with AGK, but retained the ability to bind SLC25A11.

H Subcellular fractionation assay indicated that N-ter of SMIM26 missing transmembrane domain (N1) lost the function of translocation to mitochondria.

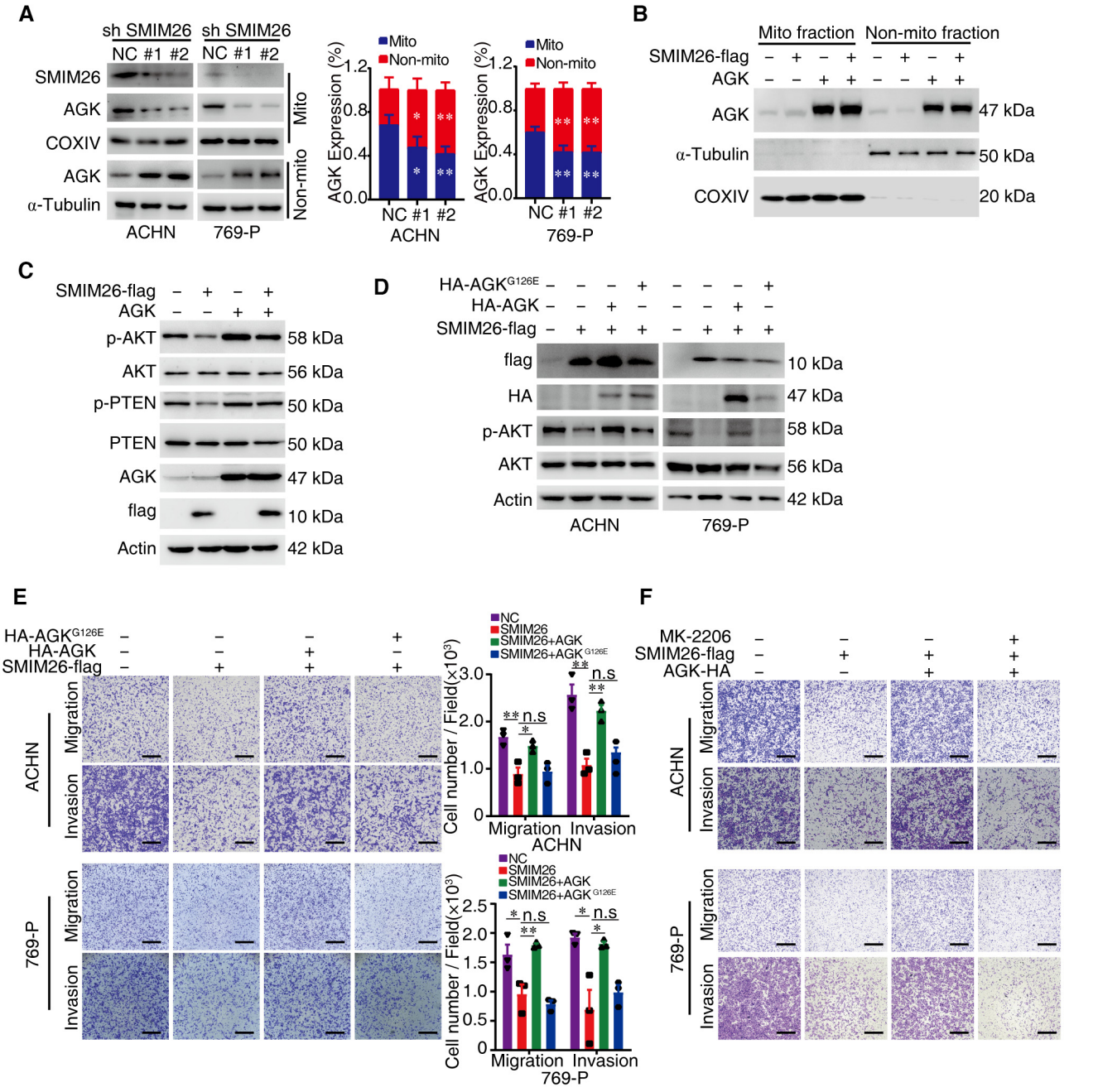

Figure EV5. SMIM26 suppressed ccRCC through the AGK/AKT pathway.

A Cellular fractionation experiments showed that silencing SMIM26 noticeably decreased the expression level of mitochondrial AGK in ACHN and 769-P cells. Data are representative of three biological replicates. Two-way ANOVA, $*P < 0.05$, $**P < 0.01$. Bars, SEM.

B Overexpression of AGK increased the mitochondrial and non-mitochondrial AGK levels in ACHN cells.

C Overexpression of AGK abrogated the SMIM26-mediated suppression of the phosphorylation of PTEN at Thr382/383 and AKT at Ser473 in ACHN cells.

D, E AGK, but not AGK^{G126E}, rescues the anti-cancer effect of SMIM26. ACHN and 769-P cells were transfected with SMIM26 and/or AGK or AGK^{G126E} as indicated. The p-AKT expression was determined by western blotting assay (D), and their migration and invasion abilities were detected by transwell assays (E). Two-way ANOVA, $*P < 0.05$, $**P < 0.01$. n.s, non-significant. Scale bar, 600 μm. Data are shown as mean ± SEM of three biological replicates.

F Transwell assays were used to test migration and invasion abilities of both ccRCC cells with indicated treatment. Scale bar, 600 μm.